

Article

Monopole and Seniority Truncations in the Large-Scale Configuration Interaction Shell Model Approach

Priyanka Choudhary and Chong Qi



Article

Monopole and Seniority Truncations in the Large-Scale Configuration Interaction Shell Model Approach

Priyanka Choudhary *  and Chong Qi * 

Department of Physics, KTH Royal Institute of Technology, 10691 Stockholm, Sweden

* Correspondence: pricho@kth.se (P.C.); chongq@kth.se (C.Q.)

Abstract: This paper addresses the challenges of solving the quantum many-body problem, particularly within nuclear physics, through the configuration interaction (CI) method. Large-scale shell model calculations often become computationally infeasible for systems with a large number of valence particles, requiring truncation techniques. We propose truncation methods for the nuclear shell model, in which angular momentum is conserved and rotational symmetry is restored. We introduce the monopole-interaction-based truncation and seniority truncation strategies, designed to reduce the dimension of the calculations. These truncations can be established by considering certain partitions based on their importance and selecting physically meaningful states. We examine these truncations for Sn, Xe, and Pb isotopes, demonstrating their effectiveness in overcoming computational limits. These truncations work well for systems with either a single type of valence nucleon or with both types. With these truncations, we are able to achieve good convergence for the energy at a very small portion of the total dimension.

Keywords: configuration interaction shell model; monopole Hamiltonian; seniority; nuclear structure



Citation: Choudhary, P.; Qi, C. Monopole and Seniority Truncations in the Large-Scale Configuration Interaction Shell Model Approach. *Symmetry* **2024**, *16*, 1685. <https://doi.org/10.3390/sym16121685>

Academic Editor: Andrea Lavagno

Received: 11 November 2024

Revised: 12 December 2024

Accepted: 16 December 2024

Published: 19 December 2024



Copyright: © 2024 by the authors. Licensee MDPI, Basel, Switzerland. This article is an open access article distributed under the terms and conditions of the Creative Commons Attribution (CC BY) license (<https://creativecommons.org/licenses/by/4.0/>).

1. Introduction

The solving of the quantum many-body problem is essential for the understanding of various microscopic systems like nuclei, atoms, and condensed matter, as well as quantum chemical multi-electron systems. In the present super-computation and machine-learning era, the importance of ab initio modelling has been repeatedly emphasized. Of all the ab initio many-body methods [1–12] that have been developed, the configuration interaction (CI) approach [13–18] may be one of the easiest to understand and most convenient to use but it is also one of the most difficult tools to implement efficiently on a supercomputer. CI involves essentially a matrix-eigenvalue equation involving an atomic or nuclear many-body Hamiltonian. One can expect to attain the exact solution of the many-body Hamiltonian if the full configuration interaction calculation involving all possible orbital bases can be carried out, which, however, is often not the case. As the dimension of the CI problem increases exponentially as the number of particles increases, in most cases one has to implement various truncation algorithms. By truncation, one aims at limiting the number of basis states for the CI model space. Unlike coupled-cluster [8–10] or many-body perturbation theory [19,20] approaches, the approximate solution of the CI after truncation can still be deemed as variational. One may be able to recover different parts of the correlation energy depending on the truncation strategy applied. Other CI approaches like the Monte Carlo shell model [21–24], variation after projection [25], and generator coordinate method [26] have also been developed to overcome the dimension difficulty, but they often started from deformed rather than spherical Slater determinants and therefore require very different algorithms.

Another important aspect to consider when designing a truncation algorithm is the possible breaking of the underlying symmetry. The restoration of the symmetry may be

quite computationally heavy. In this paper, we focus in particular on the nuclear many-body system where the angular momentum is conserved and therefore the rotational symmetry is important to restore. We will review very briefly the different truncation algorithms that have been applied in nuclear CI approaches. Then we will introduce the monopole-interaction-based importance truncation (referred to as monopole truncation) and further truncation by considering the seniority truncation as inspired by the presence of strong pairing correlation. Finally, we will test these truncations on the system that contains only one type of valence nucleon, with an equal number of valence protons and neutrons and with an unequal number of valence protons and neutrons.

The paper is divided into the following sections: In Section 2, we have briefly described the configuration interaction shell model and different shell model algorithms, focusing on the angular momentum projection in the NushellX formalism. We have proposed different truncation approaches in Section 3 in order to overcome the dimensionality issue. In Section 4, details are given about the model spaces and the effective interactions used in the present calculations. Shell model results of low-lying energy spectra with full and truncated basis states for tin, lead, and xenon isotopes are presented in Section 5. We have also calculated reduced electric quadrupole transition probability $B(E2)$ for Sn and Xe isotopes. Finally, conclusions are drawn in Section 6.

2. The Nuclear Configuration Interaction Shell Model

The CI approach is more commonly referred to as the nuclear shell model in the nuclear physics community, as it has its root in the independent particle model (the “shell model”) that was introduced 75 years ago [27–30]. The nuclear shell model has long been one of the most successful and accurate approaches in describing the nuclear structure properties. To put the nuclear shell model in a general context, one may take the independent particle model as the starting point, which may be well estimated from Hartree-Fock (HF) approaches, and the CI with effective interactions as the post-HF treatment. CI calculations can be carried out without or with assuming an inert core. The latter is more common, as the computation is often too heavy to include the core excitations and by considering the fact that the atomic nucleus is indeed characterized by strong shell effects.

A nucleus is considered to be made of interacting A -nucleons (with Z protons and N neutrons) outside a frozen inert core. The Hamiltonian for such a system of A -nucleons can be expressed in terms of single-particle energies and two-body matrix elements such as

$$H_A = T + V = \sum_{\alpha} \epsilon_{\alpha} a_{\alpha}^{\dagger} a_{\alpha} + \frac{1}{4} \sum_{\alpha \beta \gamma \delta \gamma \delta} \langle j_{\alpha} j_{\beta} | V | j_{\gamma} j_{\delta} \rangle_{JT} A_{JT:j_{\alpha} j_{\beta}}^{\dagger} A_{JT:j_{\delta} j_{\gamma}}. \quad (1)$$

where α defines a single-particle state within a given model space with the set of quantum numbers $\{n, l, j, t\}$ and the single particle energy corresponding to the state is given by ϵ_{α} . The operators a_{α}^{\dagger} and a_{α} are the creation and annihilation operators, respectively. $\langle j_{\alpha} j_{\beta} | V | j_{\gamma} j_{\delta} \rangle_{JT}$ are the antisymmetrized two-body matrix elements, and A_{JT}^{\dagger} and A_{JT} are the fermion pair creation and annihilation operators, respectively. With the above-expressed effective Hamiltonian, the eigenvalue and eigenfunctions can be calculated in the full configuration interaction shell model approach. The corresponding shell model energy of the state can be given by

$$E_{SM}^{\text{Cal.}} = \langle \Psi | H_A | \Psi \rangle \quad (2)$$

where Ψ is the calculated shell-model wave function of the state. The ground state energy can be calculated by variational methods as well, which is equivalent to the CI approach.

In practice, one commonly applies the frozen-core approximation and limits the single-particle orbitals to be the few that are just above the core orbitals (usually those within one or a few major shells). Those orbitals define the model space, while all orbitals above the model space are skipped. The single-particle energies can be taken from experimental data, HF calculations, and/or fitting to experimental data. The two-body matrix elements can be evaluated from realistic nucleon-nucleon potentials via standard perturbation theory or in-

medium Similarity Renormalization Group methods [31,32] and by fitting to experimental data [33–35]. Very often the effective Hamiltonian is provided as a list of numbers, including the single-particle energies and two-body matrix elements for a given model space. Most of the existing CI codes are designed in that way. We ignore here the three-body matrix elements. There have been recent efforts in including the three-body effects either at the mean-field (single-particle) or in explicit three-body matrix elements [36,37]. The latter is straightforward to implement in existing CI algorithms but the inclusion of three-body matrix elements can make the Hamiltonian matrix very dense and hard to handle on a supercomputer.

There are several efficient shell model codes available to construct the basis states and the Hamiltonian matrix and then solve the Hamiltonian matrix with the Lanczos [38] or similar iterative methods. Those codes are based on either angular momentum coupled J(T)-scheme (with parity, spin, and optionally isospin conserved) or uncoupled *M*-scheme (with only parity and total *M* quantum number conserved). The *M*-scheme is the de facto standard choice for large-scale calculations, as it is easier to handle on a modern computer. There are public codes in the *M*-scheme available, like BigStick [39] and KSHELL [40], both of which are highly optimized for parallel calculations on supercomputers with hybrid MPI+openMP algorithms. An *M*-scheme calculation can be implemented efficiently starting with basic bit operations where each basis (Slater determinant) can be represented as an integer. The disadvantage of the *M*-scheme is that the dimension maximizes. The dimension for a problem with certain *J* instead of *M* in the angular-momentum-coupled bases can be much smaller. The angular momentum coupling can be carried out via the coefficients of fractional parentage (cfp) [41], in multisteps [42], or through the correlated basis method re-using part of the rotationally-invariant Hamiltonian as the angular momentum projector [43].

2.1. *M*-Scheme Algorithms

The many-body Hamiltonian is invariant under rotations, which means that the total \hat{J}^2 and \hat{J}_z operators commute with the Hamiltonian. Consequently, the eigenstates of the Hamiltonian have both *J* and *M* as good quantum numbers. Because the Hamiltonian cannot connect many-body states with different *M*, it becomes advantageous to use the so-called *M*-scheme basis, where all many-body basis states share the same *M* value. This approach is particularly convenient since *M* is an additive quantum number. To determine the *M* for a Slater determinant, one can add the m_i of the occupied single-particle states. The eigenvalue can only depend upon *J*, not *M*, allowing the *M*-scheme to eliminate the rotational degeneracy and significantly reduce the size of the basis. When dealing with systems involving two types of particles, the structure of the many-body basis becomes more complicated. In such cases, the concept of factorizations is used to represent the many-body basis in order to manage this complexity.

In the case of a nucleus, we have two species of fermions, protons and neutrons. Any wavefunction can be expanded as a sum of product wavefunctions of protons and neutrons.

$$|\Psi\rangle = \sum_{\mu\nu} c_{\mu\nu} |\mu_p\rangle |\nu_n\rangle \quad (3)$$

One constructs the many-body state $|\mu_p\rangle, |\nu_n\rangle$ from a finite set of orthonormal single-particle states ϕ_i . The single-particle states must have a good quantum number as total angular momentum, *j*, and *z*-component of the angular momentum, *m*, and parity π . One can think of the single-particle states as eigenstates of a rotationally invariant single-particle Hamiltonian. For a given state ϕ_i , we need to know j_i , m_i , and π_i , where all possible m_i are allowed for a given j_i . We construct the many-body states from the single-particle states as Slater determinants using the antisymmetrized product of single-particle states.

On computers, it is convenient to represent the occupation of single-particle states using bit representations, with occupied states represented by bit 1 and unoccupied states by bit 0. This factorization makes the calculation of the many-body matrix elements of Hamilto-

nian simplified and the number of non-zero matrix elements is limited. Another M -scheme-based shell model code is KSHELL developed by N. Shimizu and collaborators [40].

2.2. Angular Momentum Projection and the NuShellX Code

The NuShellX code is one of the most popular CI codes, which gives exact eigenenergies and eigenwave functions in angular momentum coupled bases. Here, the code starts with a M -scheme basis, and the angular momentum is restored by applying a projection algorithm [44]. That hybrid algorithm was also applied in older OXBASH code [45] and our in-house code [46].

The starting point for such an algorithm is to generate a set of bases with a good magnetic quantum number in the M -scheme. Neutrons and protons can be naturally blocked into two spaces. The shell model codes ANTOINE and NATHAN [47] proposed the idea of factorization into complementary parts, which reduces the requirement of storing the many-body Hamiltonian matrix. The dimensions in the proton and neutron spaces separately are small, even for large dimensions in the total space. The bases are classified according to the distributions of particles in the single-particle orbits (referred to as partitions). Since the angular-momentum projection operator can only change the magnetic quantum number, the projection can be completed for each partition separately. Within each partition, vectors with good angular momentum can be expanded in M -scheme bases as

$$|\Psi_i^J\rangle = \sum_{m \leq i} \mathcal{M}_{im} P^J |\alpha_m\rangle, \quad (4)$$

where P^J is the projection operator and $|\alpha\rangle$ a set of specially chosen M -scheme bases. \mathcal{M} is a lower triangle matrix. Vectors with good angular momentum are the orthonormal and satisfy,

$$\begin{aligned} \langle \Psi_i^J | \Psi_j^J \rangle &= \langle \Psi_i^J | \sum_{m \leq j} \mathcal{M}_{jm} P^J |\alpha_m\rangle \\ &= \sum_{m \leq j} \mathcal{M}_{jm} \langle \Psi_i^J | \alpha_m \rangle \\ &= \delta_{ij}. \end{aligned} \quad (5)$$

Elements of \mathcal{M} can be obtained by inverting the matrix $\langle \Psi_i^J | \alpha_m \rangle$. Since the projection operator satisfies $P^J \cdot P^J = P^J$, the n -th vector can be obtained through,

$$|Q_n\rangle = |\alpha_n\rangle - \sum_{i < n} \langle O_i | \alpha_n \rangle \sum_{j \leq i} \mathcal{M}_{ij} |\alpha_j\rangle, \quad (6)$$

and

$$|\Psi_n^J\rangle = P^J |Q_n\rangle (\langle Q_n | P^J | Q_n \rangle)^{-1/2}. \quad (7)$$

For the angular momentum projection, one has the freedom to restore the total angular momentum or to do the projection separately for the proton and neutron blocks and couple them to certain total angular momentum (via standard angular momentum coupling).

The angular momentum projection can still be quite time-consuming, but it is much easier than standard cfp calculations. The advantage is that, after the projection, the dimension of the coupled bases would be much smaller, which makes it easier for the diagonalization. The disadvantage is that one has to store a large amount of angular-momentum projection coefficients either in memory [46] or on a disk as in the case of NuShellX [48]. NuShellX was written in Fortran90 by W.D.M. Rae. The proton and neutron angular momentum projections are made separately using the NuShell code, which are coupled together to make the total wave function. The NuShell is the modified version (more accurate and significantly faster) of the original JT projection code OXBASH [48]. In the version we have been developing at KTH, the code is separated into different independent codes including NuBasis (which generates the list of partitions and the M -scheme bases), NuProj which

implements the angular momentum projection and gives the J -scheme bases defined in the M -scheme bases, NuMatrix which generates the pp and nn matrices in a semi-orthogonal basis, NuOrth that completes the orthogonalization of the J -scheme matrix produced by NuMatrix, NuOper (converts the interaction into an m -scheme operator), NuOp produces a J -scheme particle-hole transformation of the np interaction, NuOpm calculates all the m -scheme operators, NuOpd converts the m -scheme operator matrix elements to reduced matrix elements in J -scheme, NuLnz (the standard Lanczos module), and NuVec that gives the eigenvectors and eigenvalues.

3. Truncation

The shell model calculations for heavy isotopes with a large number of valence particles can easily go beyond the capability of the most advanced computational resources due to the huge M -scheme dimension. A truncation criterion must be implemented in most calculations. Several works have been carried out by Horoi and co-workers [49–51] in order to develop the exponential convergence method (ECM), which reduces the whole configuration space into a subspace by concerning the average centroid of partitions. A simple and natural approach is to restrict the number of particle-hole excitations across a major shell gap or a subshell closure. It is called n-particle-n-hole truncation. If there is more than one major shell included in the model space, $n\hbar\omega$ truncation can be applied to limit the number of excitations crossing the major shells (which is often the case in no-core shell model calculations). Such truncation is easy to implement in both M -scheme and J -scheme codes, which essentially only limits the number of partitions in the calculation. All M -scheme or J -scheme bases within the kept partition are included, which avoids the symmetry break effect. Such truncation may not be very effective. Instead, in such cases, and if there is no major-shell or subshell closure, we have introduced monopole-based truncation in the shell model diagonalization method, which is described below in detail. In the present work, we have implemented the truncations in the KTH version of the popular shell model code NuShellX (where the code sources and inputs are simplified) [48].

One may design an algorithm that directly truncates the M -scheme bases. Methods like density matrix renormalization group [52–55] and importance truncation [56–59]. We have also introduced a truncation based on a pseudo-seniority-like truncation (C. Qi and N. Shimizu (unpublished.) in M -scheme [60]. The truncation in the M -scheme may, however, lead to the breaking of the rotational symmetry and the angular momentum conservation and, as a result, convergence issues.

3.1. Monopole-Based Truncation

The single-particle energy in the Hamiltonian can be deemed as the HF state energy. In principle, for a system with a large number of valence particles, one may consider starting with an HF calculation for the present shell-model Hamiltonian and re-express the two-body matrix elements in the new HF bases. There are methods developed in that or similar manners. However, it can be difficult to implement numerically, as the HF bases thus calculated may very well be deformed. Instead, the total Hamiltonian can be re-written as [61]

$$H_A = H_m + H_M. \quad (8)$$

where H_m and H_M represent the monopole and multipole Hamiltonians. The energy corresponding to the monopole Hamiltonian is expressed as

$$E_m = \langle \Psi | H_m | \Psi \rangle = \sum_{\alpha} \epsilon_{\alpha} \langle \hat{N}_{\alpha} \rangle + \sum_{\alpha \leq \beta} V_{m;\alpha\beta} \left\langle \frac{\hat{N}_{\alpha}(\hat{N}_{\beta} - \delta_{\alpha\beta})}{1 + \delta_{\alpha\beta}} \right\rangle. \quad (9)$$

In the above expression, $\sum_{\alpha} \langle \hat{N}_{\alpha} \rangle = N$ the total number of valence particles and

$$\sum_{\alpha \leq \beta} \langle \frac{\hat{N}_{\alpha}(\hat{N}_{\beta} - \delta_{\alpha\beta})}{1 + \delta_{\alpha\beta}} \rangle = \frac{N(N-1)}{2}.$$

The monopole interaction $V_{m;\alpha\beta}$ is expressed as the angular momentum weighted average value of the diagonal matrix elements for a given set of j_{α} , j_{β} , and T .

$$V_{m;\alpha\beta} = \frac{\sum_J (2J+1) \langle j_{\alpha} j_{\beta} | V | j_{\alpha} j_{\beta} \rangle_J}{\sum_J (2J+1)}. \quad (10)$$

The monopole interaction, together with the single-particle energies, determines the mean field/bulk properties of the shell-model Hamiltonian, while the residual multipole interactions are essential for the mixture of different Slater determinants and the correlation energy.

The wave function is constructed as a linear combination of all possible antisymmetric Slater determinants within a valence space. The valence space, or model space, is a set of single-particle orbitals near the Fermi surface. In the full configuration interaction shell model calculations, one needs to define the basis in terms of *partitions*. A *partition* is defined as a set of configurations with the same number of particles in each single-particle orbital. The total number of partitions for Pb isotopes with valence neutrons are presented in Ref. [62]. Then, the wave function is constructed for each partition in the $j - j$ coupled scheme or the uncoupled M scheme.

In the M -scheme, $M(j_z)$ and T_z are good quantum numbers only; angular momentum is not explicitly. It is difficult to implement the truncations, which leads to large dimensions of the bases. If we remove part of the bases within a given partition, it will create problems. Instead, it will be convenient if one includes only a limited number of partitions and considers all the M -scheme bases within a given partition. We can simply include some partitions and exclude the rest to reduce the dimension, according to their importance. We implemented an importance truncation based on the total monopole energy by taking the multipole Hamiltonian as a perturbation. The monopole energy for a given partition is written as

$$E_m^P = \langle \Psi | H_m | \Psi \rangle = \sum_{\alpha} \epsilon_{\alpha} N_{P;\alpha} + \sum_{\alpha \leq \beta} V_{m;\alpha\beta} \frac{N_{P;\alpha} (N_{P;\beta} - \delta_{\alpha\beta})}{1 + \delta_{\alpha\beta}}, \quad (11)$$

where $N_{P;\alpha}$ is the distribution of the valence particles within a given partition P . First, one needs to calculate the monopole energies for all partitions (which is carried out using Equation (11)), and all M -scheme basis states for a given partition have the same monopole energy. One needs to determine the minimum monopole energy. We defined the cutoff energy E_{cutoff} , which is the energy relative to the lowest one of all the partitions. We select the partitions whose energies are smaller than the cutoff energy and create a subspace in which the wavefunction is spanned. This truncation is referred to as “sharp cutoff truncation.” If we set the E_{cutoff} equal to its maximum value, all the partitions are taken into account, and the dimension corresponds to the full space dimension. As the cutoff energy increases, the number of configurations (partitions) included also increases, and consequently, the dimension of the subspace increases. This implies that by removing restrictions, we approach the full space calculation.

Apart from the sharp cutoff truncation, we propose an idea of the “distribution type cutoff truncation” for the first time. We consider a distribution function that is defined as

$$X = \frac{1}{1 + e((E_{\text{mono}} - E_{\text{mono_min}} - E_{\text{cutoff}})/a)},$$

where E_{mono} is the monopole energy for a particular partition, $E_{\text{mono_min}}$ and E_{cutoff} represent the minimum monopole energy and the sharp cutoff energy, respectively, and a defines

the smoothness of the distribution curve. We use a random number generator to select the bases in such a way that if the generated random number for a partition is less than the defined function X , the corresponding basis states are included; otherwise, they are excluded. The idea behind the distribution-type cutoff is to include important partitions—those excluded in the sharp cutoff monopole truncation—based on the smoothness of the function.

In the third case, we remove a part of the J -scheme bases associated with each partition based on function X . We define the allowed basis as X times the number of total bases ($X * nJT$). To check these different types of monopole-based truncations, we have performed the shell-model calculations for various isotopes. There have been attempts in the past to use an approach similar to the monopole-based truncation, and this is based on spectral distribution theory, described in Refs. [63–65].

3.2. Seniority Truncation

The seniority scheme provides a good approximation for the low-lying states of systems containing the same kind of particles [66]. This arises from the fact that monopole pairing interactions with $J = 0$ dominate the $T = 1$ two-body matrix elements. The seniority quantum number is defined as the number of unpaired nucleons in a nuclear state, i.e., the number of particles not coupled to $J = 0$. Recent works on the study of the seniority coupling scheme are reported in Refs. [67–69]. In Ref. [70], it is reported that the pairing Hamiltonian, described by the $v = 0, J = 0$ states in many shells, can provide the exact solution. These states show only a small fraction of the total wave function but represent the most significant components for describing low-lying nuclear states. Interestingly, the number of $v = 0$ states is even smaller than the total number of partitions. Alternatively, $v = 0$ states can be constructed within the M -scheme, which offers a straightforward approach. However, the dimension of the bases in such a scheme is considerably larger compared to that in the jj -scheme.

It is not trivial to define seniority in an uncoupled M -scheme or partition. Instead, we start simply with a seniority-like or quasi-seniority scheme in the M -scheme instead and define a nucleon pair as seniority (or quasi-seniority)-0 if they couple to the M quantum number $M = 0$ (of course, in practice such pairs can exhibit non-zero angular momentum and be of seniority two, strictly speaking). We hope that such configurations are the most favored components of the low-lying states, as they are expected to be dominated by low-seniority states that can be projected from those pairs. In NuShellX, a projection algorithm [44] is applied to store the angular momentum as described in Section 2.2. The angular momentum projection method [44] starts with a random M -scheme basis $|\alpha_m\rangle$ of Equation (4) on which we make an important selection. A random selection of M -scheme basis leads to a random set of J -states, which means that the eigenvectors obtained may correspond to different J values. Instead, a more effective and meaningful strategy is to begin with the basis that already has a good angular momentum J . This ensures that all the eigenvectors thus obtained have the same angular momentum. The chosen basis state should contain the most significant features about the Hamiltonian within each partition. Compared to the random projected basis used in the projection approach [44], these bases are more physically meaningful. One thus has the opportunity to perform different truncation schemes within this approach. Basis states with lower seniority are expected to play a crucial role in describing low-lying states. Ground states of even-even nuclei are generally assumed to have zero seniority (fully paired), whereas those of odd- A nuclei typically have seniority one. We implement a truncation to the selection of M states with low seniority, so that we end up with the J -states that are relevant to the ground state. We introduce the seniority quantum number (v) as $v = N - 2 * Np$, where N is the number of valence nucleons and Np the number of paired nucleons. Firstly, we check the number of nucleon pairs and determine the seniority of all M -scheme bases within each partition. For example, the M -scheme bases are 1111011 and 10001011011 in ^{202}Pb . These states have 3 and 2 pairs, respectively. Thus the respective seniority quantum numbers are 0 and 2.

Then, we identify the minimum seniority for each partition. Finally, we do the projection by selecting a starting M -state with low seniority.

Pairing correlations are anticipated to play a crucial role in describing the lowest-lying states. Generalized seniority truncation has been proposed as a truncation scheme for large-scale shell model calculations [66,71]. This approach has been applied to the Sn isotopes [72,73] and Pb isotopes, considering states with generalized seniority up to $S = 6$. The nucleon-pair approximation (NPA) is a pair-truncated shell-model approach with collective pairs as building blocks, which has been used in Refs. [74,75] for the shell model calculations. In Ref. [60], various truncation schemes for the nuclear configuration interaction shell model approach have been reported. Our method is more general, and it selects the most important partitions determined by the monopole interaction and starts with low-seniority states within that partition.

4. Model Space and the Effective Interaction

We have selected tin, xenon, and lead isotopes for the shell model study.

4.1. Lead Isotopes

For the detailed structural description of lead isotopes, we have used the interaction developed by the Stockholm group (J. Blomqvist and C. Qi (unpublished.)) [62]. For the interaction, doubly magic ^{208}Pb is assumed as the inert core. The model space is made up of six orbitals: $2p_{1/2}$, $1f_{5/2}$, $2p_{3/2}$, $0i_{13/2}$, $1f_{7/2}$, and $0h_{9/2}$ between the shell closure $N = 82 - 126$ and 353 $T = 1$ two-body matrix elements. Calculations are carried out in the hole-hole channel. The single-particle energies for the valence orbitals (relative to the $2p_{1/2}$) are as follows: $\epsilon(1f_{5/2}) = 0.570$ MeV; $\epsilon(2p_{3/2}) = 0.898$ MeV; $\epsilon(0i_{13/2}) = 1.633$ MeV; $\epsilon(1f_{7/2}) = 2.340$ MeV; $\epsilon(0h_{9/2}) = 3.414$ MeV [62]. For the selected valence space, there are 21 $T = 1$ monopole matrix elements, for which strengths are tabulated in Table 1.

Table 1. The strength of the $T = 1$ monopole matrix elements $\langle j_\alpha j_\beta | V | j_\alpha j_\beta \rangle_{J,T}$ of the pb effective interaction.

j_α	j_β	$\langle j_\alpha j_\beta V j_\alpha j_\beta \rangle_{J,T}$
$2p_{1/2}$	$2p_{1/2}$	-0.0500
$2p_{1/2}$	$1f_{5/2}$	0.0504
$2p_{1/2}$	$2p_{3/2}$	0.00625
$2p_{1/2}$	$0i_{13/2}$	0.0394
$2p_{1/2}$	$1f_{7/2}$	0.0467
$2p_{1/2}$	$0h_{9/2}$	0.0242
$1f_{5/2}$	$1f_{5/2}$	0.00833
$1f_{5/2}$	$2p_{3/2}$	0.0241
$1f_{5/2}$	$0i_{13/2}$	0.0176
$1f_{5/2}$	$1f_{7/2}$	0.0141
$1f_{5/2}$	$0h_{9/2}$	0.0886
$2p_{3/2}$	$2p_{3/2}$	-0.0913
$2p_{3/2}$	$0i_{13/2}$	0.0822
$2p_{3/2}$	$1f_{7/2}$	0.0149
$2p_{3/2}$	$0h_{9/2}$	0.0613
$0i_{13/2}$	$0i_{13/2}$	-0.00357
$0i_{13/2}$	$1f_{7/2}$	0.114
$0i_{13/2}$	$0h_{9/2}$	0.00020
$1f_{7/2}$	$1f_{7/2}$	-0.00661
$1f_{7/2}$	$0h_{9/2}$	0.0482
$0h_{9/2}$	$0h_{9/2}$	0.0923

In Ref. [62], the M -scheme dimensions for the $M^\pi = 0^+$ and the dimensions of the corresponding $J^\pi = 0^+$ states in the even-even Pb isotope are shown. In this work, the full shell model calculations for $^{194-206}\text{Pb}$ with the maximum dimension of 3.4×10^9 were carried out.

4.2. Tin and Xenon Isotopes

For the shell model calculations of tin and xenon isotopes, we have considered a model space with the neutron and proton orbitals $0g_{7/2}$, $1d_{5/2}$, $1d_{3/2}$, $2s_{1/2}$, and $0h_{11/2}$ lying between the shell closure $Z = N = 50 - 82$, assuming the doubly magic ^{100}Sn as an inert core. In this work, we have used the effective interaction derived by applying the Monte Carlo global optimization approach [76]. The effective interaction has been constructed from the realistic CD-Bonn inter-nucleon interaction [77] and renormalized by using the perturbative G-matrix approach [78]. The core-polarization effects are also taken into account in it. The mass dependence is not considered in these calculations.

There are 5 single-particle energies and 327 two-body matrix elements for the chosen interactions, 160 of which are $T = 1$ and 167 $T = 0$ elements. There are 15 $T = 1$ monopole terms, which are shown in Table 2. The single-particle energies are the same for both proton and neutron orbitals. The single-particle energies are taken relative to the $0g_{7/2}$ orbital as: $\epsilon(1d_{5/2}) = 0.172$ MeV; $\epsilon(1d_{3/2}) = 5.01279$ MeV; $\epsilon(2s_{1/2}) = 0.36906$ MeV; $\epsilon(0h_{11/2}) = 3.24863$ MeV [76]. The dimensions corresponding to $M^\pi = 0^+$ and $J_\pi = 0^+$ states in even-even Sn isotopes are shown in Ref. [76]. One can notice that the dimension grows drastically with increasing number of valence neutron numbers. The calculated results with this interaction on Sn isotopes can be found in Ref. [79].

Table 2. The strength of the $T = 1$ monopole matrix elements $\langle j_\alpha j_\beta | V | j_\alpha j_\beta \rangle_{J,T}$ of the sn100 effective interaction.

j_α	j_β	$\langle j_\alpha j_\beta V j_\alpha j_\beta \rangle_{J,T}$
$0g_{7/2}$	$0g_{7/2}$	0.000
$0g_{7/2}$	$1d_{5/2}$	-0.151
$0g_{7/2}$	$1d_{3/2}$	-0.139
$0g_{7/2}$	$2s_{1/2}$	-0.028
$0g_{7/2}$	$0h_{11/2}$	-0.261
$1d_{5/2}$	$1d_{5/2}$	-0.121
$1d_{5/2}$	$1d_{3/2}$	-0.607
$1d_{5/2}$	$2s_{1/2}$	0.203
$1d_{5/2}$	$0h_{11/2}$	-0.016
$1d_{3/2}$	$1d_{3/2}$	0.179
$1d_{3/2}$	$2s_{1/2}$	-0.768
$1d_{3/2}$	$0h_{11/2}$	-0.116
$2s_{1/2}$	$2s_{1/2}$	-0.749
$2s_{1/2}$	$0h_{11/2}$	-0.013
$0h_{11/2}$	$0h_{11/2}$	-0.244

5. Results and Discussion

5.1. The Energy Spectra of ^{202}Pb

To test the importance of monopole-based and seniority truncations, we study a simple system, ^{202}Pb , containing six valence holes. The M -scheme dimension for the ground state of ^{202}Pb is 411,184. In the first case, we apply monopole truncation with a sharp cutoff criterion in NuShellX [48]. In Figure 1, we plot the J -scheme dimensions corresponding to spins $J = 0$ to 4 as a function of energy cutoff. This figure illustrates the exponential growth of the basis states with increasing E_{cutoff} . We reach approximately 97% of the total states at an energy cutoff of 14.0 MeV, as can be seen from the figure. We have calculated the energies of the low-lying yrast positive- and negative-parity states in the truncated basis states, the convergence behavior of which is presented in Figure 2. At $E_{\text{cutoff}} = 10.0$ MeV, which includes 65% of the total basis states, we observe that convergence is nearly achieved. The calculated ground state energy with $E_{\text{cutoff}} = 10$ MeV is 0.147 MeV, which is close to the calculated energy without truncation (0.056 MeV). We found that, with increasing cutoff energy, the energies gradually converge to the full-space results. Our results are the same as those obtained from KSHELL [40].

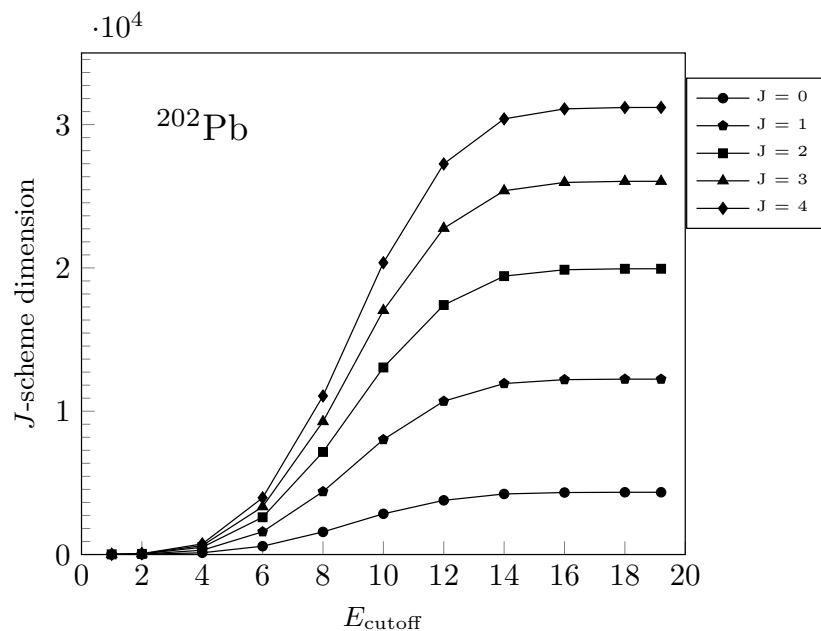


Figure 1. The J -scheme dimension for ^{202}Pb as a function of the specified cutoff energy of the monopole-based truncation for the states with $J = 0$ to $J = 4$.

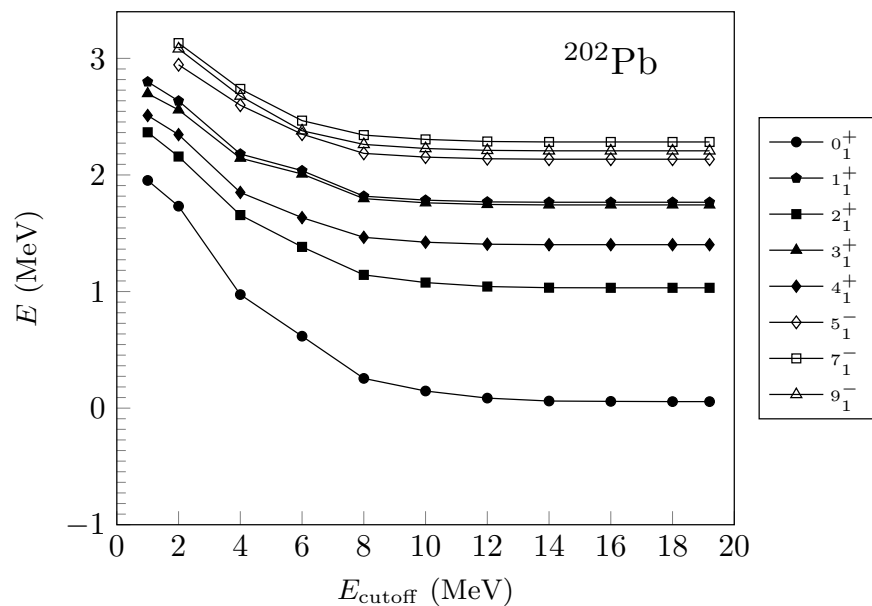


Figure 2. Convergence behaviour of the ground and yrast excited states of ^{202}Pb as a function of sharp cutoff energy.

Instead of using a sharp cutoff, we implement a distribution-type cutoff (X defined above) in monopole-based truncation for the second case. In function X , we choose a parameter value of $a = 0.5$. Whether a partition is retained or skipped depends on a random number, so each iteration of the calculation yields a different result. These results are displayed in Figure 3 with uncertainties. From the figure, it is evident that at lower energy cutoffs (below 8 MeV), the distribution-type cutoff achieves faster convergence compared to the sharp cutoff. For example, at $E_{\text{cutoff}} = 6$ MeV, the minimum energy obtained for the 0^+ state is 0.518 MeV, whereas with the sharp cutoff, the corresponding energy is 0.617 MeV.

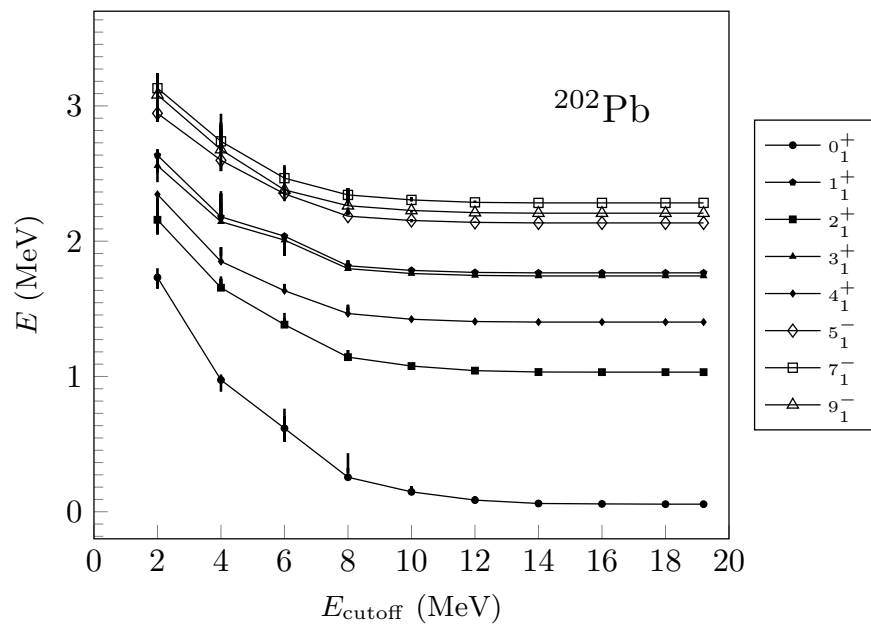


Figure 3. Shell-model energies for the yrast states in ^{202}Pb with the monopole-based truncation based on sharp cutoff energy and a distribution-type cutoff.

As described earlier, the third type of monopole-based truncation restricts the number of basis states within a given partition according to the function X . The corresponding shell-model results are shown in Figure 4a. In the figure, the solid lines represent the results obtained using a sharp energy cutoff, while the dashed red lines show the results using this third type of truncation. For the ground state, the results with the third type of truncation converge to those from the sharp cutoff at 14.0 MeV. However, for the excited states, convergence is achieved earlier, at 12 MeV. To provide a better picture, we have illustrated the convergence of the shell-model energies for the 0_1^+ , 2_1^+ , and 4_1^+ states as a function of the fraction of the J -scheme basis states considered. In Figure 4b, D represents the total number of J -scheme basis states with positive parity, while d denotes the number of basis states included in the truncated shell-model calculations.

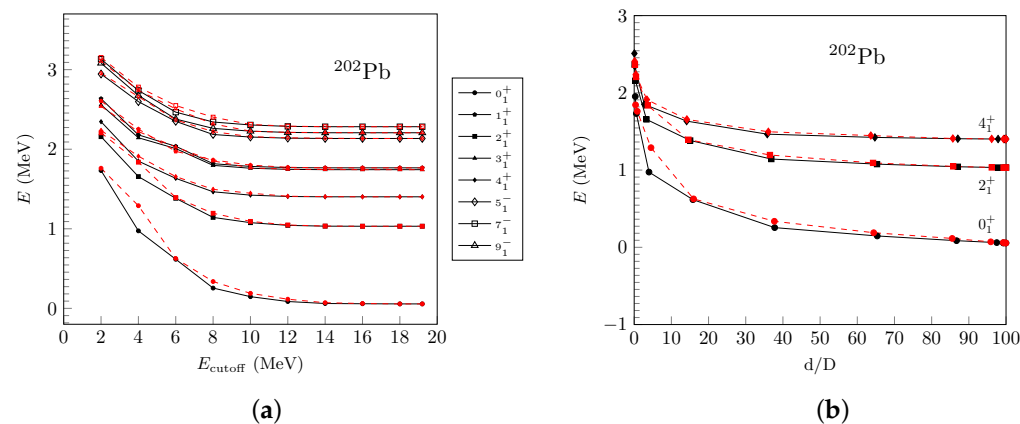


Figure 4. (a) Convergence behavior of the ground and yrast excited states of ^{202}Pb with increasing cutoff energy. (b) Convergence of the shell-model yrast energy states of ^{202}Pb with respect to the fraction of the J -scheme bases considered.

Next, we incorporate the seniority truncation on top of monopole-based truncation for the first time. As mentioned earlier, we aim to identify the most relevant basis for the ground state by taking the lower seniority states in the M -scheme. For the system

considered by us, the maximum number of unpaired nucleons is six. In our case, the M -states for a partition can have seniority quantum numbers of 0, 2, 4, and 6. We identify the minimum seniority corresponding to a partition and label it as 's.' Then, we define a function that depends on the seniority quantum number such that if the seniority for the random M -state within a partition is zero + s (minimum seniority corresponding to that partition), then that particular M -state is retained, following which, we proceed for the projection. Seniorities of $2 + s$, $4 + s$, and $6 + s$ respectively correspond to 33%, 66%, and 99% chances of generating a new basis state. In this way, we can reach a physically meaningful starting M -basis vector, which is most relevant to the ground state.

We have combined the monopole and seniority truncations in this paper for the first time. In Figure 5, we have shown the results of monopole plus seniority truncations for ^{202}Pb . Compared to the third case, we have further reduced the J -basis states based on the seniority quantum number. For minimum seniority ≤ 2 , we increase the cutoff energy by adding to it $0.5 \times$ the minimum seniority value. Accordingly, X decreases, which leads to the decrease of the J -dimension. The corresponding results are shown by dashed blue lines in Figure 5. Then, we implement the seniority truncation in the projection module to start with the M -state involving minimum seniority, and the corresponding results are shown in Figure 5 by uncertainty. It is evident from the figure that seniority truncation improves the results. As an illustration, we have displayed the convergence of the energies for the yrast 0^+ , 2^+ , and 4^+ states with an increasing number of bases in Figure 5. We can clearly see that the results obtained with monopole + seniority truncation are even better at smaller dimensions than the calculation with monopole truncation alone.

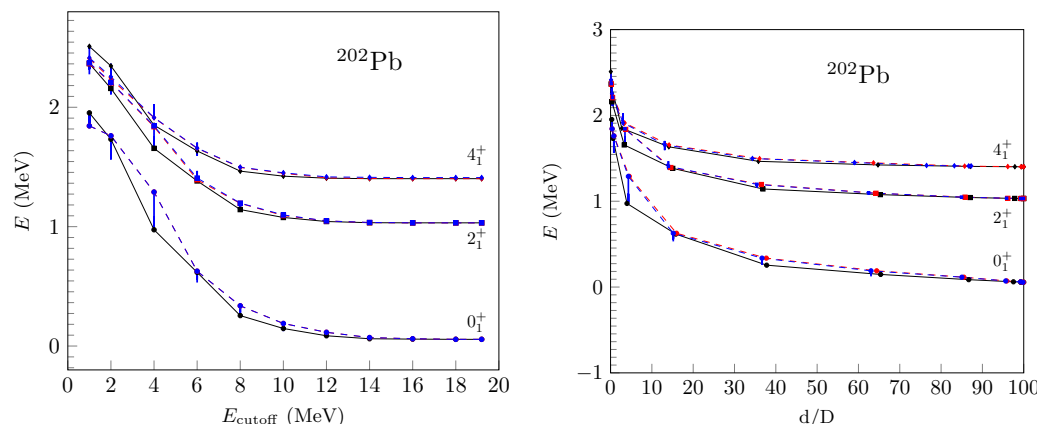


Figure 5. Shell-model energies for the low-lying states in ^{202}Pb with monopole-based plus seniority truncations as a function of cutoff energy (left) and a fraction of the bases considered (right).

5.2. The Energy Spectra and $B(E2)$ for ^{106}Sn

We have performed calculations for ^{106}Sn , 6 valence neutrons on top of the ^{100}Sn core, using the shell model with the monopole-based truncation. We have shown the J -scheme dimension with increasing cutoff energy in Figure 6. The dimension increases rapidly with increasing cutoff energy. When we include all the basis states, we obtain the full-space bases. The energies of low-lying positive-parity states with even spin are plotted in Figure 7a. As we increase cutoff energy, our truncated results approach the full-space calculation, with convergence being reached at the cutoff energy of 10 MeV. The obtained ground state energy at $E_{\text{cutoff}} = 10.0$ MeV is -6.505 MeV, while the full-space result for the same is -6.768 MeV. We noted that a very good convergence is reached with the truncated model space, even though it is only $\approx 46\%$ of the full model space.

A more stringent test for these truncations would be the calculation of the $E2$ transition strength, since quadrupole degrees of freedom are included through off-diagonal matrix elements (non-monopole term). We have calculated the $B(E2)$ value for the transition between 2_1^+ and 0^+ in ^{106}Sn ; corresponding results are shown in Figure 7b. The exper-

imentally measured $B(E2)$ value of the transition $2_1^+ \rightarrow 0_1^+$ is $0.048 e^2 b^2$ [80]. We have used the neutron effective charge $e_n^{\text{eff}} = 1.0e$ in the $B(E2)$ calculations, the same as used in Ref. [81]. The untruncated calculation gives a $B(E2)$ value of $0.027 e^2 b^2$. The discrepancy between theory and experiment might be due to missing contribution from $g_{9/2}$ orbital below $Z = 50$ shell closure [80]. Figure 7b shows that we get a converged $B(E2)$ value at small cutoff energy in ^{106}Sn .

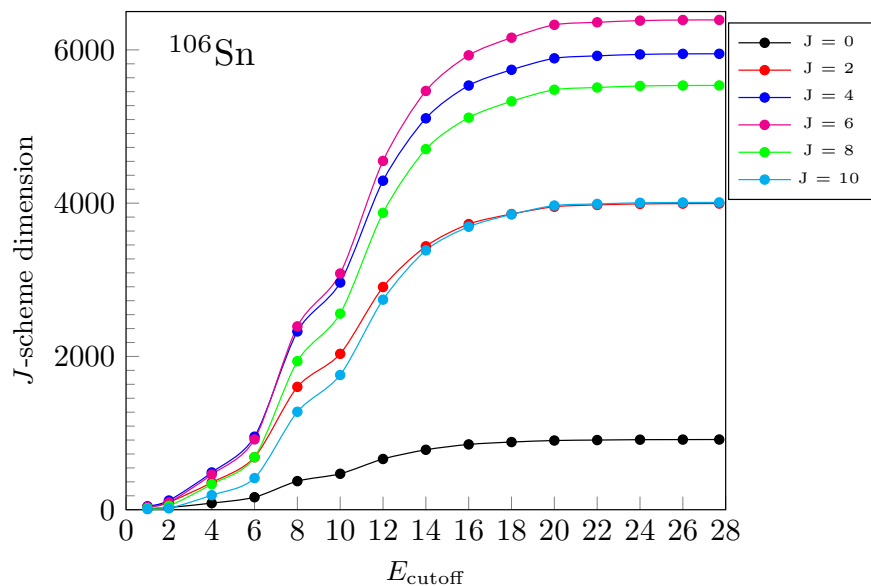


Figure 6. The J -scheme dimension for ^{106}Sn as a function of cutoff energy for the states with spins $J = 0 - 10$.

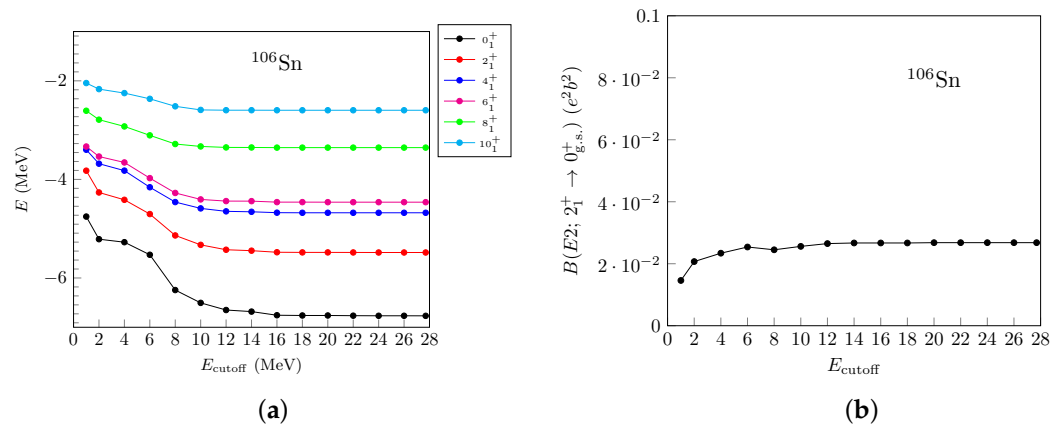


Figure 7. Convergence of (a) the shell model energies for the low-lying states and (b) the $B(E2)$ strength from the first 2^+ to 0^+ in ^{106}Sn as a function of cutoff energy.

Similar to the ^{202}Pb case, we have performed the shell model calculations for low-lying energy states with combined monopole and seniority truncations in ^{106}Sn . The results of energies are shown in Figure 8. By imposing the seniority truncation, we can obtain a faster convergence as compared to the monopole-based truncation calculation at small cutoff energy. It is clear from the figure that for the high-spin states, states with high seniority are required to get the full-space results.

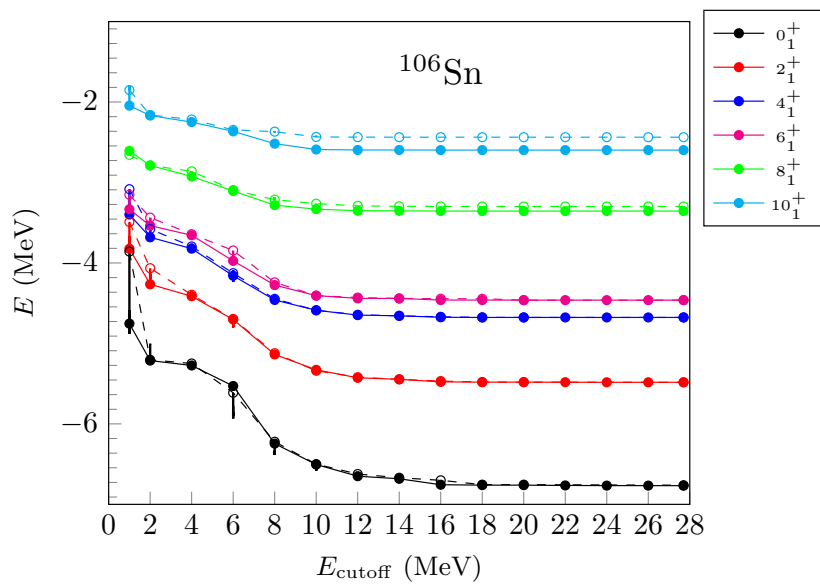


Figure 8. The shell model energies for the low-lying states in ^{106}Sn with combined monopole and seniority truncations as a function of cutoff energy.

5.3. The Energy Spectra and $B(E2)$ for ^{108}Xe

In the previous sections, we performed calculations for a system containing only one type of nucleon. Now, we aim to test the effectiveness of monopole-based truncation in a more complex system involving both protons and neutrons. For this purpose, we have done truncated calculations for the nucleus ^{108}Xe , with equal numbers of protons and neutrons ($N = Z = 54$). This nucleus is predicted to lie on the proton-drip line. Experimentally, only the ground state has been measured, which corresponds to a 0^+ state [82,83].

In our calculations, we have used the same interaction (sn100) as employed in the studies of Sn isotopes. The M -scheme dimension for the ground state of ^{108}Xe is 7.4×10^7 . In addition to the ground state, we provide predictions for the first excited 2^+ and 4^+ states, which could be useful for future experimental measurements. Figure 9a shows the calculated energies of the three lowest-lying positive parity states (0^+ , 2^+ , and 4^+) in ^{108}Xe . Without truncation, the exact energies for these states are found to be -16.377 MeV, -15.920 MeV, and -15.193 MeV, respectively. We then applied monopole-based truncation using a sharp cutoff criterion. With an energy cutoff of $E_{\text{cutoff}} = 6.0$ MeV, the calculated energies are -15.011 MeV, -14.604 MeV, and -13.978 MeV for the 0^+ , 2^+ , and 4^+ states, respectively. Calculations are then performed with $E_{\text{cutoff}} = 8.0$ MeV, which corresponds to approximately 50% of the total model space. In this case, the energies were -15.426 MeV, -14.991 MeV, and -14.323 MeV for the above-mentioned states. Remarkably, convergence is achieved using less than 20% of the full J -scheme basis, demonstrating the efficiency of the monopole-based truncation method even in systems with both types of nucleons. In Figure 9b, the convergence behavior of $B(E2)$ for the transition $2^+_1 \rightarrow 0^+_{\text{g.s.}}$ is presented with increasing cutoff energy. There is no experimental $B(E2)$ value available yet. The $B(E2)$ strength for the full-space calculation is obtained as $940.6 \text{ } e^2 \text{ fm}^4$. From the figure, it appears that convergence for $E2$ strength can be reached at a small part of the full-space basis. This indicates that the monopole-based truncation gives a well-converged value of the observables with a reduced dimension of the calculation.

In NuShellX, we have implemented the cutoff criteria separately for protons and neutrons, since projection is done separately for them. On the other hand, in KSHELL, the monopole-based truncation is made on the total monopole Hamiltonian, which contains the proton-neutron part as well. The monopole-based truncation with $E_{\text{cutoff}} = 8.0$ MeV yields the energies of -14.795 , -14.376 , and -13.761 MeV for the 0^+ , 2^+ , and 4^+ states, respectively. It indicates that, for the system with both kinds of valence nucleons, calculated

results are different from these two shell-model codes. Recently, shell model calculations have been performed for ^{200}Hg without truncation and $^{199,199}\text{Hg}$ with monopole-based truncation at $E_{\text{cutoff}} = 12$ MeV and other Hg isotopes at $E_{\text{cutoff}} = 10$ MeV using the KSHELL [84].

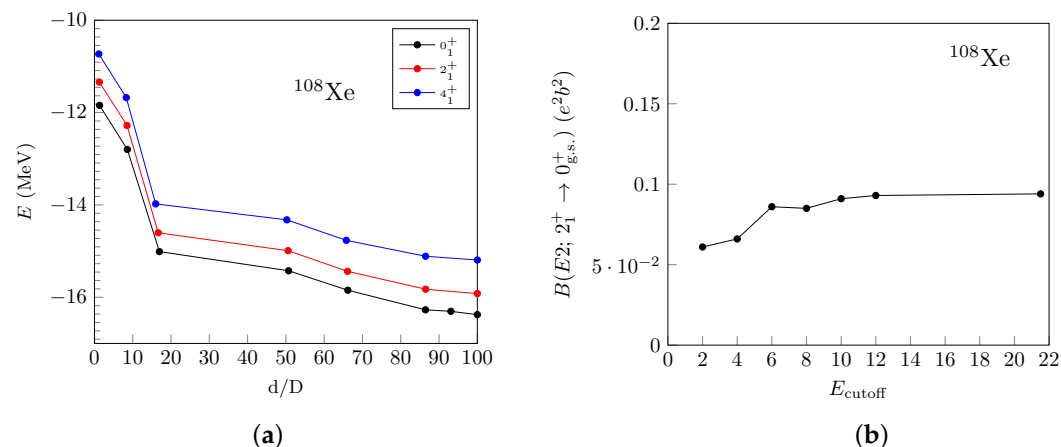


Figure 9. (a) Energies of the lowest three states of ^{108}Xe as a function of the fraction of the bases taken into consideration. (b) Calculated $B(E2)$ value for the transition $2^+_1 \rightarrow 0^+_{\text{g.s.}}$ in ^{108}Xe against the cutoff energy of the monopole truncation.

5.4. The Energy Spectra and $B(E2)$ for ^{110}Xe

We now extend our study to a more complex system, the extremely neutron-deficient $N = Z + 2$ nucleus, ^{110}Xe , which contains an unequal number of protons and neutrons (4 valence protons and 6 valence neutrons). The M -scheme dimension for the ground state of this nucleus is 1.7×10^9 , which is the maximum dimension that current shell-model codes can handle. In Ref. [85], the energies of the three lowest states in ^{110}Xe have been experimentally observed. The excitation energies of the tentative 2^+ and 4^+ states were measured to be 470 keV and 1113 keV, respectively. Interestingly, the results from Ref. [85] revealed a deviation from the normal trend of increasing energies with decreasing neutron number, which was attributed to enhanced collectivity. This anomaly is suggested to arise from the $T = 0$ neutron-proton interaction in nuclei near the $N = Z$ region.

We have performed full-space shell-model calculations using the sn100 interaction for ^{110}Xe , and the obtained energies for the lowest three states are -20.143 MeV, -19.789 MeV, and -19.141 MeV. The calculated excitation energies for the 2^+ and 4^+ states are 354 keV and 1002 keV, respectively, which show good agreement with the experimental data [85]. The calculations considering monopole-based truncation have also been performed. Figure 10 shows the convergence of the three low-lying states for ^{110}Xe as a function of the fraction of the J -scheme bases taken into account. At a cutoff energy of 2 MeV, the obtained ground state energy is -13.919 MeV. Hence, the difference between the full space calculation and the calculation with $E_{\text{cutoff}} = 2$ MeV is 6.224 MeV. For the calculation considering $\sim 37\%$ of the total dimension ($E_{\text{cutoff}} = 10$ MeV), the difference is reduced to 752 keV. With increasing cutoff energy, the energy of the ground state approaches the exact value. NuShellX gives the results of -19.391 , -19.098 , and -18.536 MeV for 0^+ , 2^+ , and 4^+ states, respectively, while the corresponding energies are -18.750 , -18.436 , and -17.887 MeV with KSHELL at $E_{\text{cutoff}} = 10.0$ MeV. The convergence is even faster when focusing solely on the spectrum relative to the ground state, as shown in Figure 10. There is a one-to-one correspondence between d/D and the cutoff energy in the left and right panels of Figure 10. The convergence is already achieved by taking only around 37% of the total bases. These calculations are significantly faster than the full space calculation. We have checked the predictive power of the monopole-based truncation by calculating the reduced $E2$ transition strength for the open-shell nucleus ^{110}Xe (with 4 valence protons and 6 valence neutrons). In Figure 11, we have plotted the $B(E2)$ between first 2^+ and 0^+ states for ^{110}Xe . Although

it is expected that achieving $B(E2)$ convergence is challenging for deformed nuclei, our results show a well-converged value is achieved at 10 MeV cutoff energy. This indicates that the monopole-based truncation with small cutoff energy is sufficient in reproducing the full-space transition strength for the open-shell nuclei.

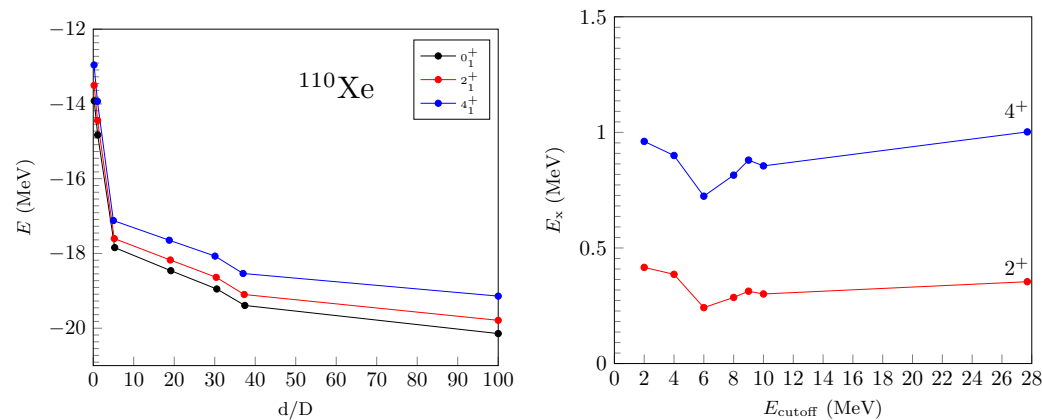


Figure 10. (Left) Energies of the lowest three states of ^{110}Xe as a function of the fraction of the bases taken into consideration. (Right) Excitation energies of first 2^+ and 4^+ states relative to the ground state as a function of E_{cutoff} .

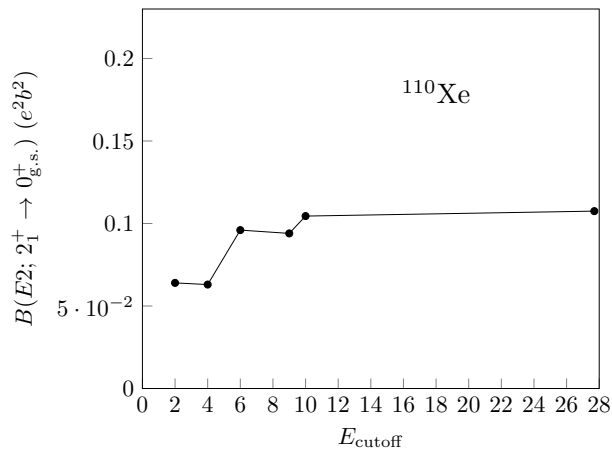


Figure 11. Convergence of the $B(E2)$ value for ^{110}Xe with the cutoff energy of the monopole-based truncation.

The monopole and seniority truncations are straightforward to implement in the shell model code. Based on the results of low-lying energy spectra and reduced $E2$ transition strength, we can conclude that these truncations are among the most efficient truncations (without breaking symmetries) for reducing the computational demands of large-scale shell-model calculations. Our results show that considering $\sim 10\text{--}30\%$ of the total dimension gives a reasonable result for both spherical and deformed nuclei. These truncations would be beneficial for the systems with many valence nucleons, allowing for feasible and accurate calculations of the nuclear structure properties.

6. Conclusions

In the present work, we have introduced two truncation techniques for the configuration interaction shell model approach to tackle the huge dimension of the Hamiltonian matrix: monopole-based truncation and seniority truncation inspired by strong pairing correlation. These truncations incorporate the selection of certain partitions according to their importance and retain M -basis states with lower seniority within each partition. As a benchmark, we have carried out large-scale shell model calculations for various systems,

including ^{106}Sn , $^{108,110}\text{Xe}$, and ^{202}Pb , comparing the calculated energies of ground and excited states and $B(E2)$ values in both truncated and full basis spaces. A good convergence is obtained with a small part of the total bases, which demonstrates the effectiveness of these truncations in reducing the dimension. These truncation methods hold promise for extending the reach of shell-model calculations to heavier nuclei, where the conventional shell model becomes computationally challenging.

Author Contributions: P.C.: Performed calculations, investigation, writing—review and editing. C.Q.: Conceptualization, methodology, investigation, writing—review and editing. All authors have read and agreed to the published version of the manuscript.

Funding: The research was funded by Olle Engkvists Foundation.

Data Availability Statement: The data generated during the current study are available on request.

Acknowledgments: The computations were enabled by resources at PDC Center for High Performance Computing, KTH Royal Institute of Technology provided by the National Academic Infrastructure for Supercomputing in Sweden (NAIIS).

Conflicts of Interest: The authors declare no conflicts of interest.

References

1. Hergert, H.; Bogner, S.; Morris, T.; Schwenk, A.; Tsukiyama, K. The In-Medium Similarity Renormalization Group: A novel ab initio method for nuclei. *Phys. Rep.* **2016**, *621*, 165–222. [\[CrossRef\]](#)
2. Stroberg, S.R.; Hergert, H.; Holt, J.D.; Bogner, S.K.; Schwenk, A. Ground and excited states of doubly open-shell nuclei from ab initio valence-space Hamiltonians. *Phys. Rev. C* **2016**, *93*, 051301. [\[CrossRef\]](#)
3. Parzuchowski, N.M.; Stroberg, S.R.; Navrátil, P.; Hergert, H.; Bogner, S.K. Ab initio electromagnetic observables with the in-medium similarity renormalization group. *Phys. Rev. C* **2017**, *96*, 034324. [\[CrossRef\]](#)
4. Stroberg, S.R.; Henderson, J.; Hackman, G.; Ruotsalainen, P.; Hagen, G.; Holt, J.D. Systematics of $E2$ strength in the sd shell with the valence-space in-medium similarity renormalization group. *Phys. Rev. C* **2022**, *105*, 034333. [\[CrossRef\]](#)
5. Pieper, S.C.; Pandharipande, V.R.; Wiringa, R.B.; Carlson, J. Realistic models of pion-exchange three-nucleon interactions. *Phys. Rev. C* **2001**, *64*, 014001. [\[CrossRef\]](#)
6. Pervin, M.; Pieper, S.C.; Wiringa, R.B. Quantum Monte Carlo calculations of electroweak transition matrix elements in $A = 6, 7$ nuclei. *Phys. Rev. C* **2007**, *76*, 064319. [\[CrossRef\]](#)
7. Marcucci, L.E.; Pervin, M.; Pieper, S.C.; Schiavilla, R.; Wiringa, R.B. Quantum Monte Carlo calculations of magnetic moments and $M1$ transitions in $A \leq 7$ nuclei including meson-exchange currents. *Phys. Rev. C* **2008**, *78*, 065501. [\[CrossRef\]](#)
8. Jansen, G.R.; Engel, J.; Hagen, G.; Navratil, P.; Signoracci, A. Ab Initio Coupled-Cluster Effective Interactions for the Shell Model: Application to Neutron-Rich Oxygen and Carbon Isotopes. *Phys. Rev. Lett.* **2014**, *113*, 142502. [\[CrossRef\]](#)
9. Hagen, G.; Papenbrock, T.; Dean, D.J.; Hjorth-Jensen, M. Ab initio coupled-cluster approach to nuclear structure with modern nucleon-nucleon interactions. *Phys. Rev. C* **2010**, *82*, 034330. [\[CrossRef\]](#)
10. Hagen, G.; Hjorth-Jensen, M.; Jansen, G.R.; Papenbrock, T. Emergent properties of nuclei from ab initio coupled-cluster calculations. *Phys. Scr.* **2016**, *91*, 063006. [\[CrossRef\]](#)
11. Barrett, B.R.; Navrátil, P.; Vary, J.P. Ab initio no core shell model. *Prog. Part. Nucl. Phys.* **2013**, *69*, 131–181. [\[CrossRef\]](#)
12. Epelbaum, E.; Krebs, H.; Lee, D.; Meißner, U.G. Ab Initio Calculation of the Hoyle State. *Phys. Rev. Lett.* **2011**, *106*, 192501. [\[CrossRef\]](#) [\[PubMed\]](#)
13. SHAVITT, I. The history and evolution of configuration interaction. *Mol. Phys.* **1998**, *94*, 3–17. [\[CrossRef\]](#)
14. Brussaard, P.J.; Glaudemans, P.W.M. *Shell-Model Applications in Nuclear Spectroscopy*; North-Holland Publishing Company: Amsterdam, The Netherlands, 1977.
15. Caurier, E.; Martínez-Pinedo, G.; Nowacki, F.; Poves, A.; Zuker, A.P. The shell model as a unified view of nuclear structure. *Rev. Mod. Phys.* **2005**, *77*, 427–488. [\[CrossRef\]](#)
16. Brown, B.A.; Wildenthal, B.H. Status of the Nuclear Shell Model. *Annu. Rev. Nucl. Part. Sci.* **1988**, *38*, 29–66. [\[CrossRef\]](#)
17. Tsunoda, Y.; Otsuka, T. Configuration Interaction Approach to Atomic Nuclei: The Shell Model. In *Handbook of Nuclear Physics*; Tanihata, I., Toki, H., Kajino, T., Eds.; Springer Nature: Singapore, 2020; pp. 1–49. [\[CrossRef\]](#)
18. Heyde, K. *From Nucleons to the Atomic Nucleus: Perspectives in Nuclear Physics*; Springer: Berlin/Heidelberg, Germany, 1998.
19. Roth, R.; Langhammer, J. Padé-resummed high-order perturbation theory for nuclear structure calculations. *Phys. Lett. B* **2010**, *683*, 272–277. [\[CrossRef\]](#)
20. Tichai, A.; Arthuis, P.; Duguet, T.; Hergert, H.; Somà, V.; Roth, R. Bogoliubov many-body perturbation theory for open-shell nuclei. *Phys. Lett. B* **2018**, *786*, 195–200. [\[CrossRef\]](#)
21. Honma, M.; Mizusaki, T.; Otsuka, T. Diagonalization of Hamiltonians for Many-Body Systems by Auxiliary Field Quantum Monte Carlo Technique. *Phys. Rev. Lett.* **1995**, *75*, 1284–1287. [\[CrossRef\]](#) [\[PubMed\]](#)

22. Otsuka, T.; Honma, M.; Mizusaki, T. Structure of the $N = Z = 28$ Closed Shell Studied by Monte Carlo Shell Model Calculation. *Phys. Rev. Lett.* **1998**, *81*, 1588–1591. [\[CrossRef\]](#)

23. Shimizu, N. Recent Progress of Shell-Model Calculations, Monte Carlo Shell Model, and Quasi-Particle Vacua Shell Model. *Physics* **2022**, *4*, 1081–1093. [\[CrossRef\]](#)

24. Shimizu, N.; Mizusaki, T. Variational Monte Carlo method for shell-model calculations in odd-mass nuclei and restoration of symmetry. *Phys. Rev. C* **2018**, *98*, 054309. [\[CrossRef\]](#)

25. Gao, Z.C. Variation after projection calculations for high-spin states. *Phys. Lett. B* **2022**, *824*, 136795. [\[CrossRef\]](#)

26. Lin, W.; Zhou, E.; Yao, J.; Hergert, H. Quantum-Number Projected Generator Coordinate Method for ^{21}Ne with a Chiral Two-Nucleon-Plus-Three-Nucleon Interaction. *Symmetry* **2024**, *16*, 409. [\[CrossRef\]](#)

27. Mayer, M.G. On Closed Shells in Nuclei. *Phys. Rev.* **1948**, *74*, 235–239. [\[CrossRef\]](#)

28. Mayer, M.G. On Closed Shells in Nuclei. II. *Phys. Rev.* **1949**, *75*, 1969–1970. [\[CrossRef\]](#)

29. Haxel, O.; Jensen, J.H.D.; Suess, H.E. On the “Magic Numbers” in Nuclear Structure. *Phys. Rev.* **1949**, *75*, 1766. [\[CrossRef\]](#)

30. Mayer, M.G. Nuclear Configurations in the Spin-Orbit Coupling Model. I. Empirical Evidence. *Phys. Rev.* **1950**, *78*, 16–21. [\[CrossRef\]](#)

31. Kuo, T.; Brown, G. Structure of finite nuclei and the free nucleon-nucleon interaction: An application to ^{18}O and ^{18}F . *Nucl. Phys.* **1966**, *85*, 40–86. [\[CrossRef\]](#)

32. Honma, M.; Otsuka, T.; Brown, B.A.; Mizusaki, T. Effective interaction for pf-shell nuclei. *Phys. Rev. C* **2002**, *65*, 061301. [\[CrossRef\]](#)

33. Cohen, S.; Kurath, D. Effective interactions for the 1p shell. *Nucl. Phys.* **1965**, *73*, 1–24. [\[CrossRef\]](#)

34. Brown, B.A.; Richter, W.A. New “USD” Hamiltonians for the sd shell. *Phys. Rev. C* **2006**, *74*, 034315. [\[CrossRef\]](#)

35. Yuan, C.; Suzuki, T.; Otsuka, T.; Xu, F.; Tsunoda, N. Shell-model study of boron, carbon, nitrogen, and oxygen isotopes with a monopole-based universal interaction. *Phys. Rev. C* **2012**, *85*, 064324. [\[CrossRef\]](#)

36. Cole, B.; Watt, A.; Whitehead, R. Three-body forces and shell-model binding energies. *Phys. Lett. B* **1975**, *57*, 24–26. [\[CrossRef\]](#)

37. Andreozzi, F.; Sartoris, G. Effective three-body interactions in the $f_{7/2}$ shell. *Nucl. Phys. A* **1976**, *270*, 388–398. [\[CrossRef\]](#)

38. Lanczos, C. An iteration method for the solution of the eigenvalue problem of linear differential and integral operators. *J. Res. Natl. Bur. Stand. Sect. B* **1950**, *45*, 255–282. [\[CrossRef\]](#)

39. Johnson, C.W.; Ormand, W.E.; Krastev, P.G. Factorization in large-scale many-body calculations. *Comput. Phys. Commun.* **2013**, *184*, 2761–2774. [\[CrossRef\]](#)

40. Shimizu, N.; Mizusaki, T.; Utsuno, Y.; Tsunoda, Y. Thick-restart block Lanczos method for large-scale shell-model calculations. *Comput. Phys. Commun.* **2019**, *244*, 372–384. [\[CrossRef\]](#)

41. deShalit, A.; Talmi, I. *Nuclear Shell Theory*; Dover: Mineola, NY, USA, 1963.

42. Xu, Z.; Qi, C.; Blomqvist, J.; Liotta, R.; Wyss, R. Multistep shell model description of spin-aligned neutron–proton pair coupling. *Nucl. Phys. A* **2012**, *877*, 51–58. [\[CrossRef\]](#)

43. Jiao, L.F.; Sun, Z.H.; Xu, Z.X.; Xu, F.R.; Qi, C. Correlated-basis method for shell-model calculations. *Phys. Rev. C* **2014**, *90*, 024306. [\[CrossRef\]](#)

44. LÖWDIN, P.O. Angular Momentum Wavefunctions Constructed by Projector Operators. *Rev. Mod. Phys.* **1964**, *36*, 966–976. [\[CrossRef\]](#)

45. Langanke, K.; Maruhn, J.A.; Koonin, S.E. (Eds.) *Computational Nuclear Physics 1: Nuclear Structure*; Springer: Berlin/Heidelberg, Germany, 1991. [\[CrossRef\]](#)

46. Qi, C.; Xu, F.R. Modern shell-model diagonalizations with realistic NN forces. *arXiv* **2007**, arXiv:nucl-th/0701036. [\[CrossRef\]](#)

47. Caurier, E.; Nowacki, F. Present Status of Shell Model Techniques. *Acta Phys. Pol. B* **1999**, *30*, 705.

48. Rae, W.D.M. NuShellX. Available online: <http://www.garsington.eclipse.co.uk/> (accessed on 20 October 2023).

49. Horoi, M.; Brown, B.A.; Zelevinsky, V. Truncation method for shell model calculations. *Phys. Rev. C* **1994**, *50*, R2274–R2277. [\[CrossRef\]](#)

50. Horoi, M.; Volya, A.; Zelevinsky, V. Chaotic Wave Functions and Exponential Convergence of Low-Lying Energy Eigenvalues. *Phys. Rev. Lett.* **1999**, *82*, 2064. [\[CrossRef\]](#)

51. Horoi, M.; Brown, B.A.; Zelevinsky, V. Applying the exponential convergence method: Shell-model binding energies of $0f_{7/2}$ nuclei relative to ^{40}Ca . *Phys. Rev. C* **2002**, *65*, 027303. [\[CrossRef\]](#)

52. Dukelsky, J.; Pittel, S.; Dimitrova, S.S.; Stoitsov, M.V. Density matrix renormalization group method and large-scale nuclear shell-model calculations. *Phys. Rev. C* **2002**, *65*, 054319. [\[CrossRef\]](#)

53. Pittel, S.; Sandulescu, N. Density matrix renormalization group and the nuclear shell model. *Phys. Rev. C* **2006**, *73*, 014301. [\[CrossRef\]](#)

54. Rotureau, J.; Michel, N.; Nazarewicz, W.; Płoszajczak, M.; Dukelsky, J. Density Matrix Renormalization Group Approach for Many-Body Open Quantum Systems. *Phys. Rev. Lett.* **2006**, *97*, 110603. [\[CrossRef\]](#)

55. Tichai, A.; Knecht, S.; Kruppa, A.; Legeza, Ö.; Moca, C.; Schwenk, A.; Werner, M.; Zarand, G. Combining the in-medium similarity renormalization group with the density matrix renormalization group: Shell structure and information entropy. *Phys. Lett. B* **2023**, *845*, 138139. [\[CrossRef\]](#)

56. Andreozzi, F.; Iudice, N.L.; Porrino, A. An importance sampling algorithm for generating exact eigenstates of the nuclear Hamiltonian. *J. Phys. G Nucl. Part. Phys.* **2003**, *29*, 2319. [\[CrossRef\]](#)

57. Stumpf, C.; Braun, J.; Roth, R. Importance-truncated large-scale shell model. *Phys. Rev. C* **2016**, *93*, 021301. [\[CrossRef\]](#)

58. Bianco, D.; Andreozzi, F.; Lo Iudice, N.; Porrino, A.; Dimitrova, S. An upgraded version of an importance sampling algorithm for large scale shell model calculations. *J. Phys. Conf. Ser.* **2010**, *205*, 012002. [\[CrossRef\]](#)

59. Coraggio, L.; Gargano, A.; Itaco, N. Double-step truncation procedure for large-scale shell-model calculations. *Phys. Rev. C* **2016**, *93*, 064328. [\[CrossRef\]](#)

60. Qi, C. Seniority and truncation schemes for the nuclear configuration interaction approach. *Rom. J. Phys.* **2015**, *60*, 782–791.

61. Poves, A.; Zuker, A. Theoretical spectroscopy and the fp shell. *Phys. Rep.* **1981**, *70*, 235–314. [\[CrossRef\]](#)

62. Qi, C.; Jia, L.Y.; Fu, G.J. Large-scale shell-model calculations on the spectroscopy of $N < 126$ Pb isotopes. *Phys. Rev. C* **2016**, *94*, 014312. [\[CrossRef\]](#)

63. Wong, S.S.M. Truncation of the nuclear shell-model space using spectral strength distribution. *Nucl. Phys. A* **1978**, *295*, 275–288. http://inis.iaea.org/search/search.aspx?orig_q=RN:09377946. [\[CrossRef\]](#)

64. Wong, S.S.M. *Nuclear Statistical Spectroscopy*; Oxford University Press: New York, NY, USA, 1986.

65. Chang, F.S.; French, J.B.; Thio, T.H. Distribution methods for nuclear energies, level densities, and excitation strengths. *Ann. Phys.* **1971**, *66*, 137. [\[CrossRef\]](#)

66. Talmi, I. *Simple Models of Complex Nuclei: The Shell Model and Interacting Boson Model*; Beitrage zur Wirtschaftsinformatik; Harwood Academic Publishers: Reading, UK, 1993.

67. Qi, C.; Wang, X.B.; Xu, Z.X.; Liotta, R.J.; Wyss, R.; Xu, F.R. Alternate proof of the Rowe-Rosensteel proposition and seniority conservation. *Phys. Rev. C* **2010**, *82*, 014304. [\[CrossRef\]](#)

68. Qi, C. Partial conservation of seniority in the $j = 9/2$ shell: Analytic and numerical studies. *Phys. Rev. C* **2011**, *83*, 014307. [\[CrossRef\]](#)

69. Qi, C.; Xu, Z.; Liotta, R. Analytic proof of partial conservation of seniority in $j = 9/2$ shells. *Nucl. Phys. A* **2012**, *884–885*, 21–35. [\[CrossRef\]](#)

70. Xu, Z.X.; Qi, C. Shell evolution and its indication on the isospin dependence of the spin–orbit splitting. *Phys. Lett. B* **2013**, *724*, 247–252. [\[CrossRef\]](#)

71. Jia, L.Y. Practical calculation scheme for generalized seniority. *J. Phys. G Nucl. Part. Phys.* **2015**, *42*, 115105. [\[CrossRef\]](#)

72. Jia, L.Y.; Qi, C. Generalized-seniority pattern and thermal properties in even Sn isotopes. *Phys. Rev. C* **2016**, *94*, 044312. [\[CrossRef\]](#)

73. Maheshwari, B.; Jain, A.K.; Singh, B. Asymmetric behavior of the $B(E2\uparrow; 0^+ \rightarrow 2^+)$ values in $^{104–130}\text{Sn}$ and generalized seniority. *Nucl. Phys. A* **2016**, *952*, 62–69. [\[CrossRef\]](#)

74. Jiang, H.; Qi, C.; Lei, Y.; Liotta, R.; Wyss, R.; Zhao, Y.M. Nucleon pair approximation description of the low-lying structure of $^{108,109}\text{Te}$ and ^{109}I . *Phys. Rev. C* **2013**, *88*, 044332. [\[CrossRef\]](#)

75. Jiang, H.; Lei, Y.; Qi, C.; Liotta, R.; Wyss, R.; Zhao, Y.M. Magnetic moments of low-lying states in tin isotopes within the nucleon-pair approximation. *Phys. Rev. C* **2014**, *89*, 014320. [\[CrossRef\]](#)

76. Qi, C.; Xu, Z.X. Monopole-optimized effective interaction for tin isotopes. *Phys. Rev. C* **2012**, *86*, 044323. [\[CrossRef\]](#)

77. Machleidt, R. High-precision, charge-dependent Bonn nucleon-nucleon potential. *Phys. Rev. C* **2001**, *63*, 024001. [\[CrossRef\]](#)

78. Hjorth-Jensen, M.; Kuo, T.T.; Osnes, E. Realistic effective interactions for nuclear systems. *Phys. Rep.* **1995**, *261*, 125–270. [\[CrossRef\]](#)

79. Available online: <http://www.nuclear.kth.se/cqi/sn100/> (accessed on 14 April 2024).

80. Vaman, C.; Andreoiu, C.; Bazin, D.; Becerril, A.; Brown, B.A.; Campbell, C.M.; Chester, A.; Cook, J.M.; Dinca, D.C.; Gade, A.; et al. $Z = 50$ Shell Gap near ^{100}Sn from Intermediate-Energy Coulomb Excitations in Even-Mass $^{106–112}\text{Sn}$ Isotopes. *Phys. Rev. Lett.* **2007**, *99*, 162501. [\[CrossRef\]](#)

81. Banu, A.; Gerl, J.; Fahlander, C.; Górska, M.; Grawe, H.; Saito, T.R.; Wollersheim, H.-J.; Caurier, E.; Engeland, T.; Gniady, A.; et al. ^{108}Sn studied with intermediate-energy Coulomb excitation. *Phys. Rev. C* **2005**, *72*, 061305. [\[CrossRef\]](#)

82. Möller, P.; Mumpower, M.; Kawano, T.; Myers, W. Nuclear properties for astrophysical and radioactive-ion-beam applications (II). *At. Data Nucl. Data Tables* **2019**, *125*, 1–192. [\[CrossRef\]](#)

83. Data Extracted Using the NNDC World Wide Web Site from the ENSDF. Available online: <https://www.nndc.bnl.gov/ensdf/> (accessed on 10 September 2024).

84. Sahoo, S.; Srivastava, P.C.; Shimizu, N.; Utsuno, Y. Nuclear structure properties of $^{193–200}\text{Hg}$ isotopes within large-scale shell model calculations. *Phys. Rev. C* **2024**, *110*, 024306. [\[CrossRef\]](#)

85. Sandzelius, M.; Hadinia, B.; Cederwall, B.; Andgren, K.; Ganioglu, E.; Darby, I.G.; Dimmock, M.R.; Eeckhaudt, S.; Grahn, T.; Greenlees, P.T.; et al. Identification of Excited States in the $T_z = 1$ Nucleus ^{110}Xe : Evidence for Enhanced Collectivity near the $N = Z = 50$ Double Shell Closure. *Phys. Rev. Lett.* **2007**, *99*, 022501. [\[CrossRef\]](#)

Disclaimer/Publisher’s Note: The statements, opinions and data contained in all publications are solely those of the individual author(s) and contributor(s) and not of MDPI and/or the editor(s). MDPI and/or the editor(s) disclaim responsibility for any injury to people or property resulting from any ideas, methods, instructions or products referred to in the content.